

Title: Automated Detection and Spatio-Temporal Classification of Semi-Arid Channel Networks

Authors:

- 1) Mukesh Kumar
Graduate Student
212 Sackett Bldg.
Dept. of Civil and Environmental Engineering
Penn State University, University Park, 16802
muk139@psu.edu
- 2) Gopal Bhatt
Graduate Student
212 Sackett Bldg.
Dept. of Civil and Environmental Engineering
Penn State University, University Park, 16802
cxdl1@psu.edu
- 2) Peter Beeson
Graduate Student
212 Sackett Bldg.
Dept. of Civil and Environmental Engineering
Penn State University, University Park, 16802
cxdl1@psu.edu
- 2) Christopher J. Duffy (Corresponding Author)
Professor
212 Sackett Bldg.
Dept. of Civil and Environmental Engineering
Penn State University, University Park, 16802
cxdl1@psu.edu

1 **Abstract**

2 Identification of the spatial distribution of ephemeral, intermittent and perennial channel
3 networks over large ungauged basins in semi-arid regions is an important step for
4 hydrodynamic simulation, landscape evolution and riparian vegetation dynamics, and
5 calibration of watershed models. This paper describes an automated method for detection
6 of stream channels and their classification into ephemeral, intermittent and perennial
7 reaches using ASTER Level 1B remote sensing data. The methodology involves
8 calculation of normalized difference water index map of the area of interest followed by
9 bi-level uni-modal thresholding to obtain the wet channel network. This step is repeated
10 over a registered set of multi-temporal images followed by application of a change-
11 detection algorithm to obtain a classified map of the channel network with reaches of
12 different water retention time scales.

13 *Keywords:* Normalized Difference Water Index; automated image thresholding;
14 Ephemeral channels; remote sensing; change detection; hydrology.

16 **1. Introduction**

17 Remotely-sensed spatio-temporal classification of river networks according to the
18 water retention time scale associated with each perennial, intermittent or ephemeral
19 channel reach can provide an important tool for eco-hydrologic analysis and modeling.
20 This channel reach classification into perennial, intermittent or ephemeral reaches (*PIE*)
21 has traditionally been used to characterize or describe the conditions for: surface-
22 groundwater interaction (Michaelides *et. al.*, 2002), the riparian vegetation growth and

1 redistribution (Rood *et. al.*, 2003), channel geomorphologic changes (Canfield *et. al.*
2 2005), and aquatic life support (Rosario and Resh, 2000). In semi-arid regions of the
3 American southwest, which is largely unguaged and where intermittent and ephemeral
4 reaches are the primary surface hydrologic features, it is important to identify the spatial
5 distribution of *PIE* for proper accounting of spatially distributed water budgets and
6 understanding of ecological and geo-morphological interaction between channel and its
7 surroundings. Spatial *PIE* maps in unguaged basins are particularly useful as a “control
8 base map” for verification of distributed hydrologic models.

9 The local hydrodynamic interactions between channel and the aquifer are different
10 within each *PIE* category. Transmission losses from an ephemeral channel to deep water
11 table are often a rapid transient process produced by an infiltration impulse from a
12 convective storm (Besbes *et al.*, 1978; Freyberg, 1983; Razzak and Seytoux, 1983).
13 Losses or gains in a perennial channel reach are generally more slowly varying or even
14 quasi-steady in larger perennial rivers. Existence of a particular type of stream reach is
15 controlled by the local hydrogeology, ground and bedrock topography and its location in
16 regional groundwater flow field (Toth, 1962). In, the semi-arid basins of southwest such
17 as the Rio Grande valley of central New Mexico, perennial channels may exist at high
18 elevation where the runoff ratio (R/P) tends to be high due to orographic effects. At lower
19 elevation R/P is very low and channel reaches are either intermittent or ephemeral. Using
20 the definitions of the USGS, perennial river-reaches support flow round the year,
21 intermittent streams are seasonal and ephemeral streams flow only in direct response to
22 precipitation (USGS, 2008). At all elevations the water table plays a key role. During the
23 summer monsoon, intermittent stream may gain water from the aquifer while drying and

1 losing water and flow when the water table drops below the stream bed. Intermittent wet
2 patches in the dried channel network can also exist due to hydrogeologic anomaly in the
3 river bed due to clay lenses, reduced aquifer thicknesses (Sahuquillo, 2004) or where
4 shallow bed rock - caused by faulting or uplift - limits the depth of groundwater storage.
5 Taken together *PIE* classification can help to determine the time scale and thus the
6 processes creating streamflow in complex river networks of the southwest US.

7 High resolution spatio-temporal data obtained from remote sensing has emerged as
8 an important resource in the mapping of fluvial systems and fluvial networks (Mertes,
9 2002), and this is particularly true in ungaged basins. This study focuses on an automated
10 technique to process remotely sensed images for identification of channel reaches with
11 different time scales. In the first step, a categorical image depicting the regions in the
12 channel reaches that are wet or dry at any one point in time is obtained. The next step
13 involves using a temporally distributed series of such categorical images to perform pixel-
14 wise change detection. Information fusion from change detection results is used to finally
15 generate a classification map of the channel reaches based on their varied time scales. The
16 obtained classified map has been validated using a conceptual geo-topographic framework
17 and a steady state distributed hydrologic model simulation.

18

19 **2. Study Area**

20 The study has been conducted in lower semi-arid Rio Salado (drainage area = 3575
21 km²) basin around Sevilleta Long Term Ecological (Sevilleta LTER) research station in
22 New Mexico. Perennial and Intermittent reaches in Rio Salado are the primary source of
23 ground water recharge in this watershed. The Rio Salado also has a very large sediment

1 contribution to the Rio Grande (Simcox, 1983). Near the Rio Grande riparian corridor,
2 the Rio Salado crosses a Long Term Ecological Research station (<http://sev.lternet.edu/>)
3 dedicated to understanding riparian dynamics in a semi-arid region (Beeson and Duffy,
4 2004; Wyckoff *et. al.*, 2004; Vivoni *et. al.*, 2005; Passel *et. al.*, 2003 and Winter *et. al.*,
5 2005). The main source of streamflow in the Rio Salado is due to summer thunderstorms
6 and to a lesser degree winter precipitation. Historical daily stream flow measurements at
7 San Acacia (a USGS gauging station, ID = 08354000) on Rio Salado suggests that Rio
8 Salado flows for an average of only 10.6% days of the year. The stream is typically wet
9 or flowing only during the months of July, August and September. Fig. 1 shows the daily
10 streamflow and the percentage of time for which the stream remains dry each month. The
11 geographical extent of the area (of size 1150 km²) is shown in Fig. 2.

13 **3. Data**

14 Remotely sensed data obtained by the Advanced Spaceborne Thermal Emission and
15 Reflection Radiometer (ASTER) on board NASA's Terra spacecraft has been used in this
16 study. ASTER covers a wide spectral region with 14 bands from the visible to the thermal
17 infrared with high spatial, spectral and radiometric resolution. The spatial resolution
18 varies with wavelength: 15 m in the visible and near-infrared (VNIR), 30 m in the short
19 wave infrared (SWIR), and 90 m in the thermal infrared (TIR). Each ASTER scene
20 covers an area of 60 x 60 km. Detailed descriptions about ASTER data can be found in
21 Fujisada *et. al.* (1998). ASTER level 1b data (which is radiometrically and geometrically
22 corrected) was obtained from <http://edcimswww.cr.usgs.gov/pub/imswelcome/>. The
23 multispectral nature and high spatial and temporal resolution of the ASTER data is

1 reasonably suited for the surface feature identification, image classification and
2 interpretations used in this study (Jinlong *et. al.*, 2003). The strategy proposed in this
3 paper is generic and can be applied to data from other Earth Observing Satellites (EOS)
4 multispectral sensors like MODIS. However, it should be mentioned that we expect that
5 results could be improved if data with higher spatio-temporal resolution were available.
6 Fig. 2 shows a false colored composite of the area of interest used in the present study.
7 We note that only cloud-free cotemporaneous data have been used in this analysis.

8

9 **4. Approach**

10 The multi-step automated strategy applied in this study is depicted in Fig. 3. The
11 primary step is image rectification to correct the geometric distortions arising during
12 acquisition process such as due to platform instability and viewing geometry. The step is
13 particularly important when multi-temporal images need to be compared on *per-pixel*
14 basis to track changes.

15 *4.1. Image Rectification*

16 ASTER Level-1B data has embedded metadata with geo-registration details
17 which include: map projection, datum, rotation angle and cell size. However, we observe
18 that a shift as large as 500m in X-direction and 50m in Y-direction exists between
19 georegistered multi-temporal images. The error is pointed out (as a red dot) in a
20 representative co-registered set of images in Fig. 4. This geometric error is mainly
21 because of nutation and error in referencing of earth ellipsoid (NASA-EOS team, email
22 communication, 2005). This unsystematic error is corrected by performing rectification,
23 geocoding and warping (Pratt, 1991) using ground control points (GCPs). These GCPs

1 are matched to the true coordinates on the ground by computing a transformation matrix
2 followed by resampling. Nearest-neighbor resampling strategy is used so as to not
3 introduce any new pixels.

4 4.2 Image Processing

5 Using the geo-registered multitemporal images, wetness of each pixel is evaluated
6 by calculating a normalized difference water index map (NDWI).

7 4.2.1. Normalized Difference Water Index

8 NDWI (Gao, 1996) is a quantitative measure of liquid water content (Jackson et. al.,
9 2003) and is defined by

$$10 \quad NDWI = \frac{R_{SWIR} - R_{NIR}}{R_{NIR} + R_{SWIR} + \varepsilon} \quad (1)$$

11 where R_{SWIR} and R_{NIR} is the reflectance in a short wave infrared wavelength and near
12 infrared wavelength channels respectively and ε is a small number to avoid
13 indeterminate (denominator equal to zero) calculations. The index was first used for
14 Landsat TM/ETM+ data where R_{NIR} and R_{SWIR} correspond to bands 4 (0.78 – 0.90 μm)
15 and 5(1.55 – 1.75 μm) respectively. Buhe *et. al.*, 2004 used the same index to map
16 moisture distribution in the watershed using ASTER Level 1B data. The R_{NIR} and R_{SWIR}
17 bands used in ASTER NDWI calculation are bands 3N (0.78 – 0.86 μm) and 6 (2.185 –
18 2.225 μm). We note that the spatial resolution of band 3N and band 6 are 15m and 30m
19 respectively. Band 6 is resampled to 15m resolution. Though this step does not add any
20 extra information to band 6, it does leaves band 3N at its original finer resolution during
21 further processing. The NDWI values can be easily interpreted from the spectral
22 signature of common land-cover types depicted in Fig. 5. Notably, there is a significant

1 difference in the percentage reflectance level of green vegetation at wavelengths
2 corresponding to the two bands in consideration. On the other hand the difference in the
3 reflectance in bands 3N and 6 is far smaller for water and bare soil with respect to that for
4 vegetation. NDWI for wet regions on the ground (channels or lake) have smaller
5 (positive) values relative to the background. Characteristic NDWI for vegetated regions is
6 large negative values. The NDWI map obtained is renormalized from 0 to 1. Areas in the
7 scene with higher water content will have values closer to 1. Next we perform the
8 automated image classification for wet and dry pixel sets.

9 *4.2.2 Automated Thresholding*

10 Multispectral digital classification (Zhu and Blumberg, 2002; Aynekulu et. al., 2008),
11 where an image scene is divided into a number of groups each representing a particular
12 land-cover type on the ground, is carried out using supervised, unsupervised or hybrid
13 classifiers (Schowengerdt, 1983; Lillesand, 1987). Supervised classification methods
14 such as maximum-likelihood classifier need ground truth information (Strahler, 1980)
15 and are based on the assumption of normality for pixel distribution in classes.
16 Unsupervised methods like k-means clustering are semi-automated and need smaller a
17 degree of user input to classify the images. Here we use an automated and efficient
18 histogram-based, bi-level thresholding algorithm to segment the NDWI image into wet
19 and dry pixels.

20 The thresholding technique automatically selects an optimal pixel value for
21 separating objects of interest in an image from the background based on the frequency
22 distribution of pixels in the image. Most of the existing thresholding techniques use the
23 histogram of the image to select a good threshold. The histogram of an image is the
24 frequency distribution of grey levels in that image. If in the image the objects have

1 significantly different grey values from the background, the histogram will exhibit two
2 different peaks with a valley in-between. Such a histogram is called a bimodal histogram
3 and the determination of a suitable threshold value is a relatively simple matter. Several
4 threshold selection methods including those based on entropy (Kapur *et. al.*, 1985; Pun,
5 1980; Dizenzo *et. al.*, 1998), moment preservation (Tsai, 1985) and error minimization
6 (Kittler and Illingworth, 1986; Chan *et. al.*, 1998) are found to work best for the cases
7 with distinct modes in image intensity histogram. Incidentally, the NDWI maps obtained
8 from the previous step produces a histogram where one of the modes is much larger than
9 the other and its contribution effectively stymies the other class, resulting in a unimodal
10 histogram. The large peak obtained in the unimodal histogram is because of the
11 background response from classes such as a fairly vegetated or a bare soil. This uni-
12 modality of the histogram however poses difficulty in selection of threshold.

13 For bi-level segmentation of NDWI images, a unimodal thresholding algorithm is
14 needed. A number of unimodal thresholding algorithms like LMedS method, Poisson
15 method, Connectivity method and Corner method (Gorman, 1994; Rosin, 1999) have
16 been investigated by Rosin *et. al.*, (2000). For this study, a unimodal thresholding
17 technique by Rosin, 2001 which is more robust and accurate is employed. This algorithm
18 assumes that there is only one relatively large peak. A straight line is drawn from the
19 peak of the histogram to its end. The selected threshold pixel value is the one that
20 maximizes the perpendicular distance between the line joining peak and end of the
21 histogram to the histogram itself. The perpendicular distance from any pixel value on the
22 histogram location (x_i, y_i) to the line $(x_1, y_1) \leftrightarrow (x_2, y_2)$ is given by:

$$d_i = \frac{(y_1 - y_2)x_i - (x_1 - x_2)y_i - x_2y_1 + x_1y_2}{\sqrt{(x_1 - x_2)^2 + (y_1 - y_2)^2}} \quad (2)$$

1
2
3 The value of x_i for which the distance d_i is maximum is the required threshold. Threshold
4 calculation of an image scene (AST_L1B_003_06162002175757_07052002124606) is
5 shown in Fig. 6. This threshold divides the image into two classes. The resulting
6 segmented image for ASTER scene
7 (AST_L1B_003_06162002175757_07052002124606) is shown in Fig. 7. Note that the
8 two classes obtained by thresholding are a “dry” class which corresponds to areas below
9 threshold and a “wet-water” class corresponding to the regions which are above threshold
10 value. The “wet-water” class contains both the wet pixels and the watered pixels. Fig. 7
11 shows the wet-water class. For visual interpretation only have we divided the wet-water
12 class into two clusters using a Jenk’s optimal segmentation algorithm (Coulson, 1987 and
13 Jenks, 1977). As expected, water pixels form linear features for the most part correspond
14 to stream channels. We note that a large, relatively wet region is observed in the scene
15 shown in Fig. 7, which is in part due to a convective precipitation event that happened a
16 day before the scene was taken. The wet pixels also include pixels with temporary
17 ponding and near-surface ground water along smaller tributaries and gullies that are wet
18 for limited period after the large storm. Such wet regions show up as narrow dotted linear
19 features in Silver Creek, Popotosa Canada and Jencia Creek. The wet region lying along
20 the Rio Grande to its western side in the lower half of Fig. 7 represents irrigation
21 diversions, channels and drains in agricultural land.

22 Next we focus on the water retention time scales and classification of stream
23 reaches within the Rio Salado channel network.

1 4.3. Delineation of Stream Network from Digital Elevation Model (DEM)

2 Flow network delineation in a watershed is a standard DEM processing step
3 which is based on finding the direction of maximum slope for each DEM cell. The flow
4 direction information is used to derive all the upstream cells that contribute flow to a
5 particular cell. Cells with a large flow accumulation (support) value denote the streams.
6 Several methods exist to extract a drainage network from the flow accumulation (O'
7 Callaghan and Mark (1984), Quinn *et. al.*, 1991; Tarboton, 1997). Here we use what is
8 referred to as the D8 algorithm to obtain the drainage network (Tarboton, 1997).

9 Along each possible stream reach candidate, a buffer area of 100 m on the either
10 side is identified (shown in Fig. 7). This limits the analysis to those regions of the
11 thresholded NDWI map which are candidates for further study (e.g. likely channels).
12 Next we detect changes in wet-dry pixels over time, and trace the pixels that remain
13 dry/wet all the time or for a shorter period.

14 4.4. Change Detection

15 Comparison of two or more than two satellite images acquired at different times
16 can be used to evaluate the changes on the ground. Several studies on change detection
17 for environmental monitoring have been carried out (Zoran and Anderson, 2006; Singh,
18 1989; Jensen, 1996; Rynzar and Wagner, 2001). The two common change detection
19 approaches are – a) “pre-classification” and “post-classification”. The first approach
20 involves simultaneous analysis of multi-temporal images to find the differences in
21 spectral reflectance with time. This method assumes that the changes in spectral values in
22 the multi-temporal images are due to the changes on the ground. However, these changes
23 can also be because of variations in atmospheric conditions when the images are taken, or

1 because of variations in solar illumination angles or sensor calibration trends. So the
2 multi-temporal satellite images are normalized radiometrically to a common radiometric
3 level before any further processing is performed on them (Du *et. al.*, 2001). This is
4 followed by thresholding to mark the regions which actually underwent significant
5 changes (Eastman and Mackendry, 1994). The second approach avoids the problems
6 associated with radiometric correction by tracking changes in the sequence of image
7 which are already categorical in nature, like the ones which have been obtained by
8 thresholding in Section 4.2. Thresholded images are categorical as they are divided into
9 two categories viz. “wet-water” and “dry”. The latter approach avoids any need for
10 image renormalization.

11 Categorical image change detection involves tracking the change in each pixel
12 over different periods.

13 *4.5. Information fusion*

14 Change-detected information for each categorical image with respect to the base
15 image is documented and fused to form a final classified map. The flow chart in Fig. 8
16 depicts the fusion strategy. If a water pixel changes to a dry pixel or a dry pixel changes
17 to a water pixel, it is marked “Intermittent”. If the water pixels don’t undergo change,
18 they are marked “perennial” and if the “dry” pixels don’t undergo any change, they are
19 marked “ephemeral”. “Ephemeral” regions in the channel respond fast to storms and they
20 dry off quickly too because of infiltration and evaporation. We note that most pixels
21 appear to be dry in most of the images. This behavior is characteristic of this region, as
22 most of the higher order streams are ephemeral. We also note that the cloud-free images
23 used in this study didn’t have a precipitation event within 24 hours of the image

1 acquisition. The final fused map showing intermittent and perennial regions are shown in
2 Fig. 9(b).

3

4 **5. Results**

5 The final classified map according to three different time scales is shown in Fig. 10. Here
6 we have only geocoded the classified information obtained in previous section to the
7 stream network. Although we have a limited number of cloud-free remotely sensed
8 images available to test the multi-temporal change detection, the results still produce a
9 reasonable fused map and a product suitable for application to model and process studies.
10 From Fig. 10, we see that most of the reaches in the main channel, upper Rio-Grande, has
11 larger time scales as it is filled with water all the year round. However its tributary, the
12 Rio Salado is ephemeral in most regions. Next we validate our results with ancillary
13 hydro-geologic information, historical data, and hydrologic modeling. We identify four
14 different reaches (inside square boxes) on Rio Salado (shown in Fig. 10). Reach 4 is
15 ephemeral while reach 1, 2 and 3 are intermittent/ ephemeral. The spatial distribution is
16 validated using two approaches:

17 *5.1. Qualitative Validation*

18 We observe that the distribution of water retention time scale in the river reach
19 correlates to the geologic structure along Rio Salado, which is shown in Fig. 11. At
20 region 1 and region 2 and 3, the impermeable crystalline bedrock and impermeable
21 volcanic rocks respectively are shallow. This reduces the aquifer storage depth and
22 supports “ponding”. The low infiltration rate of the shallow bedrock prevents leakage of

1 water. In comparison to that, region 4 falls in the alluvium sediment region where water
2 infiltrates fast after storms letting this channel section dry.

3 *5.2. Quantitative Validation*

4 A steady state distributed model simulation of Rio Salado Watershed using
5 ModHMS model (Panday and Huyakorn, 2004; Beeson, 2008) was performed. The
6 steady state model provides a long term hydrologic water balance within the watershed,
7 as well as the average surface water depths. The long-term average net recharge of 0.5
8 inches/day obtained from various locations (NCDC COOP stations) in the vicinity of the
9 watershed was uniformly applied. Simulated head in the channel network shows
10 distributed pattern of wet and dry reaches as shown in Fig. 12. Comparing Fig. 12 and 10,
11 we observe that the spatial distribution of ephemeral/intermittent spots obtained from
12 thresholding and change detection of remote sensing images closely resemble the wet
13 reaches obtained from steady state simulations. We note that the model simulation was
14 performed only for lower Rio Salado.

15

16 **6. Conclusions**

17 An automated procedure for classification of channel network into regions with different
18 time scale of water retention is implemented. Multi-temporal data set is georegistered
19 and then automatic uni-modal thresholding is performed to obtain the regions which are
20 wet and dry. Using a buffer around the stream reaches, an area of the watershed that is
21 used for change detection is selected. Change detection in the multi-temporal thresholded
22 images with respect to a base image is derived. Information regarding this change is
23 fused to obtain a classified map of the drainage network showing regions with different

1 time scales. The results are validated using a conceptual geologic network and steady
2 state ModHMS model simulation (Beeson, 2008).

3

4 **References**

- 5 Aynekulu, E., Kassawmar, T. & Tamene, L. (2008). Applicability of ASTER imagery in
6 mapping land use cover as a basis for biodiversity studies in drylands of northern
7 Ethiopia. *Afr. J. Ecol.*, 46 (Suppl. 1): 19–23
- 8 Beeson, P., & Duffy, C. (2004). Geodatabase development in support of integrated
9 hydrologic forecasting for an ungauged ephemeral channel: Rio Salado, *American*
10 *Geophysical Union*, Spring Conference, Montreal, Canada.
- 11 Beeson, P. (2008). *Integrated hydrologic forecasting for an ungauged ephemeral*
12 *watershed: Rio Salado, New Mexico*. PhD Thesis. Penn State University.
- 13 Buhe, A., Kaneko, M., Shimada, S., & Tsuchiya, K. (2004). Estimating soil moisture in
14 the arid and semi-arid region using Terra/ASTER data, *Proceeding of International*
15 *Symposium on Participatory Strategy for Soil and Water Conservation*, 2004.
- 16 Canfield, H.E., Lane, L.J., Wilson, C.J., Crowell, K.J., & Thomas, W.A. (2005).
17 Modeling scour and deposition in ephemeral channels after wildfire. *Catena*. 61(2-3):
18 273-291.
- 19 Chan, F.H.Y., Lam, F.K., & Zhu, H. (1998). Adaptive thresholding by variational
20 method. *IEEE Transactions on Image Processing* 7 (3), 468– 473.
- 21 Coulson, M. R. C. (1987). In the matter of class intervals for choropleth maps: With
22 particular reference to the work of George F. Jenks: *Cartographica*, v. 24, p. 16-39

1 Dizenzo, S., Cinque, L., & Levialdi, S. (1998). Image thresholding using fuzzy entropies.
2 *IEEE Transactions on Systems, Man and Cybernetics*. B 28 (1), 15–23.

3 Du, Y., Cihlar, J., Beaubien, J. & Latifovic, R. (2001). Radiometric normalization,
4 compositing and quality control for satellite high resolution image mosaics over large
5 areas. *IEEE Trans. Geosci. Remote Sens.*, 39(3): 623-634.

6 Eastman, J.R., & McKendry, J.E. (1994). Change and time series analysis. *Explorations*
7 *in GIS Technology*, vol. 1. UNITAR, Geneva, Switzerland.

8 Fujisada, H., Sakuma, F., Ono, A., & Kudoh, M. (1998). Design and preflight
9 performance of ASTER Instrument protoflight model. *IEEE Transactions on Geoscience*
10 *and Remote Sensing*, 36, 1152– 1160.

11 Gao, B. (1999). NDWI – a normalized difference water index for remote sensing of
12 vegetation liquid water from space. *Remote Sensing of Environment*, 58, 257-266.

13 Gorman, L.O. (1994) Binarization and Multithresholding of document images using
14 connectivity. *CVGIP Graphical Models and Image Processing*, vol. 56, No. 6, pp. 494-
15 506.

16 Goodrich, D.C., Lane, L.J., Shillito, R.A., Miller, S.N., Syed, K.H., & Woolhiser. D.A.
17 (1997). Linearity of basin response as a function of scale in a semi-arid watershed. *Water*
18 *Resources Research* 33(12):2951- 2965.

19 Jackson, T.J., Chen, D., Cosh, M., Li, F., Anderson, M., Walthall, C., Doriaswamy, P., &
20 Hunt, E.R.. (2004). Vegetation water content mapping using Landsat data derived
21 normalized difference vegetation index for corn and soybeans. *Remote Sensing of*
22 *Environment*, 92, 475-482.

- 1 Jenks, G.F. (1977). Optimal data classification for choropleth maps. *Occasional paper*
2 *No. 2*, Department of geography, University of Kansas, Lawrence.
- 3 Jensen, J. R. (1996). *Introductory Digital Image Processing: A Remote Sensing*
4 *Perspective*, Second Edition. Prentice Hall, 316 p.
- 5 Jinlong, F., Bingfang, W., & Huiping, H., (2003). Comparative Assessment of ASTER
6 Image and ETM+ Fusion Image for Agricultural Applications, , 4, 2203-2205.
7 *Geoscience and Remote Sensing Symposium*, 2003. IGARSS '03.
- 8 Kapur, J.N., Sahoo, P.K., & Wong, A.K.C. (1985). A new method for gray-level picture
9 thresholding using the entropy of the histogram. *Graphical Models and Image*
10 *Processing*, 29: 273-285.
- 11 Kittler, J., & Illingworth, J. (1986). Minimum error thresholding. *Pattern Recognition*,
12 19: 41-47
- 13 Lillesand, T. M. & Kiefer, R. W. (1987). Remote Sensing and Image Interpretation, *John*
14 *Wiley & Sons, Inc.*
- 15 Maidment, D. R., ed. (2002), *Arc Hydro Gis for Water Resources*, ESRI Press, Redlands,
16 CA, 203 p.
- 17 Michaelides, K., & Wainwright, J. (2002). Modeling the effects of hillslope-channel
18 coupling on catchment hydrologic response, *Earth Surface Processes and Landforms*, 27:
19 1441-1457
- 20 O'Callaghan, J. F., & Mark, D. M. (1984). The Extraction of Drainage Networks from
21 Digital Elevation Data. *Computer Vision, Graphics and Image Processing*, 28: 328-344.

1 Panday, S., & Huyakorn. P. S. (2004). A fully coupled physically-based spatially-
2 distributed model for evaluating surface/subsurface flow. *Advances in Water Resources*
3 27:361-382.

4 Passel, H.D., Tidwell, V.C., Conrad, S.H., Thomas, R.P., & Roach. J. (2003).
5 <http://www.sandia.gov/water/docs/ModelingSANDrprtFINAL.pdf>, (Accessed on July 03,
6 2005).

7 Pratt, W. K., *Digital Image Processing*, 2nd edition, pp.430-440, John Wiley & Sons,
8 1991.

9 Pun, T. 1980. A New Method for Gray-Level Picture Threshold Using the Entropy of the
10 histogram. *Signal Processing*, 2(3): 223-237.

11 Quinn, P., Beven, K., Chevallier, P., & Planchon, O. (1991). The Prediction of Hillslope
12 Flow Paths for Distributed Hydrological Modeling Using Digital Terrain Models.
13 *Hydrological Processes*, 5: 59-80.

14 NASA-EOS Team. (2005). “ the reason for these offsets is because of disparate pointing
15 angles of the scenes. To compound the problem, there are some geometric errors
16 (nutation – related longitudinal error, earth ellipsoid –related terrain error and an earth
17 rotation angle error) which are yet to be accurately fixed”.

18 Rood, S.B., Braatne, J.H., & Hughes. F.M.R. (2003). Ecophysiology of riparian
19 cottonwoods: streamflow dependency, water relations and restoration. *Tree Physiology*
20 23: 1113-1124

21 Rosario, R.B. & Resh, V.H. (2000). Invertebrates in intermittent and perennial streams: Is
22 the hyporheic zone a refuge from drying? *Journal of the North American Benthological*
23 *Society*. 19(4): 680-696.

1 Rosin, P.L. (1999), Unimodal Thresholding, *2nd Conf. Image Analysis*, 1999, pp. 585-592
2

3 Rosin, P.L., Herva's, J., & Barredo, J.I. (2000). Remote sensing image thresholding for
4 landslide motion detection. *Proc. 1st Int. Workshop on Pattern Recognition Techniques*
5 *in Remote Sensing*, Andorra, 10– 17.

6 Rosin, P.L. (2001). Unimodal thresholding, *Pattern Recognition*, vol. 34, no. 11, pp.
7 2083-2096.

8 Ryznar, R. M., & Wagner, T. W. (2001). Using Remotely Sensed Imagery to Detect
9 Urban Change: Viewing Detroit From Space. *Journal of the American Planning*
10 *Association*, 67(3):327-336.

11 Sahuquillo.(2004). [http://www.iucn.org/places/medoffice/CD2004/conten/doc2004/
12 HydroGeo_Paper_Eph_Rivers.pdf](http://www.iucn.org/places/medoffice/CD2004/conten/doc2004/HydroGeo_Paper_Eph_Rivers.pdf) . (Accessed on July 03, 2005).

13 Sevilleta LTER, <http://sev.lternet.edu/>, (Accessed on July 03, 2005).

14 Schowengerdt, R. A. (1983). *Techniques for Image Processing and Classification in*
15 *Remote Sensing*, Academic Press, Inc.

16 Simcox, A. C. (1983). The Rio Salado at flood. In New Mexico Geological Society
17 guidebook, *39th annual field conference, Socorro Region II*, ed. by Charles E. Chapin,
18 pp. 325–327, Socorro, New Mexico.

19 Singh, A. (1989). Digital change detection techniques using remotely-sensed data.
20 *International Journal of Remote Sensing*, 10(6):989-1003.

21 Strahler, A.H. (1980). The use of prior probabilities in maximum likelihood classification
22 of remote sensing data., *Remote sensing of Environment*, 10, 135-163, 1980.

1 Tarboton, D. G. (1997). A New Method for the Determination of Flow Directions and
2 contributing Areas in Grid Digital Elevation Models. *Water Resources Research*, 33(2):
3 309-319.

4 Tsai W.H. (1985). Moment-preserving thresholding: A new approach" *Graphical Models*
5 and Image Processing, 19: 377-393

6 USGS. (2008). <http://water.usgs.gov/wsc/glossary.html>

7 Vivoni, E.R., Bowman, R.S., Wyckoff, R.L., Jakubowski, R. T. & Richards, K.E. (2005).
8 Analysis of a Monsoon Flood Event in an Ephemeral Tributary to the Río Grande and Its
9 Downstream Hydrologic Effects. *Water Resources Research*.

10 Winter, C.L., Fort, D.M., Conrad, K., Kreiner, D., Cooper, D., & Greene, R. Water
11 resources of upper Rio Grande basin: History, Hydrology and Management,
12 <http://www.lanl.gov/projects/chinawater/documents/wrriogrande.pdf>, (Accessed on July
13 03, 2005).

14 Wyckoff, R., Vivoni, E.R. & Rinehart, A. (2004). Fine-Resolution Hydrologic Modeling
15 of Semiarid River Basins: Preliminary Results from Upper Rio Grande Subbasins.
16 *American Geophysical Union*, Fall Conference, San Francisco, CA.

17 Zhu, G. & Blumberg, D.G., (2002). Classification using ASTER data and SVM
18 algorithms: the case study of Beer Sheva, Israel, *Remote Sens. Environ.* 80, 233-240.

19 Zoran, M. & Andersona, E. (2006). The use of multi-temporal and multispectral satellite
20 data for change detection analysis of the Romanian Black Sea coastal zone, *Journal of*
21 *Optoelectronics and Advanced Materials*, 8(1), 252-256

22

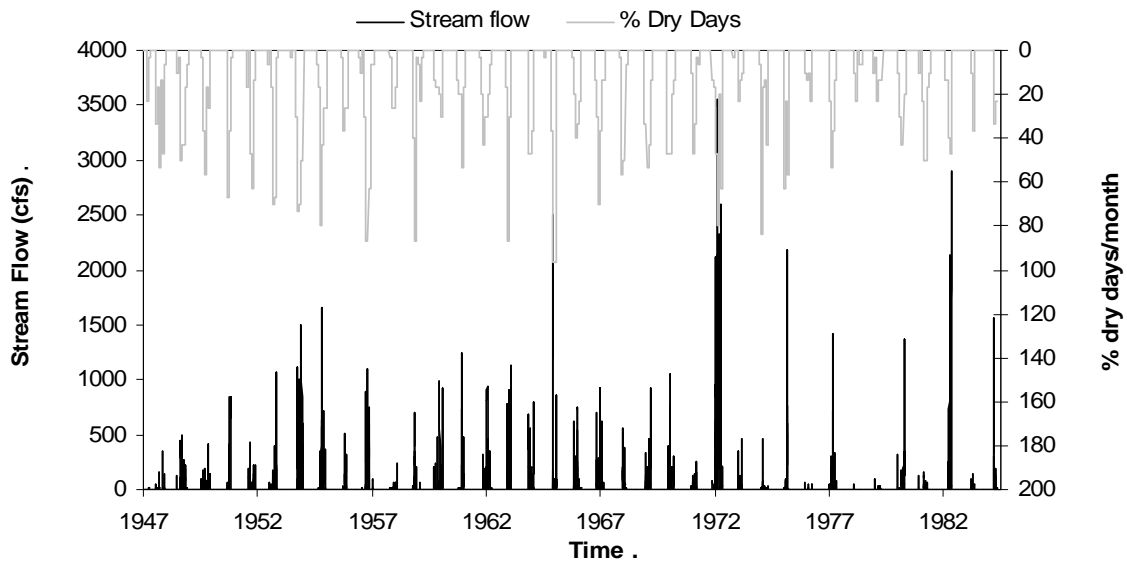


Fig. 1: Streamflow time series at Rio Salado near San Acacia (USGS Station ID: 08354000). On daily basis, the stream remains dry 89 % of the year.

DRAFT

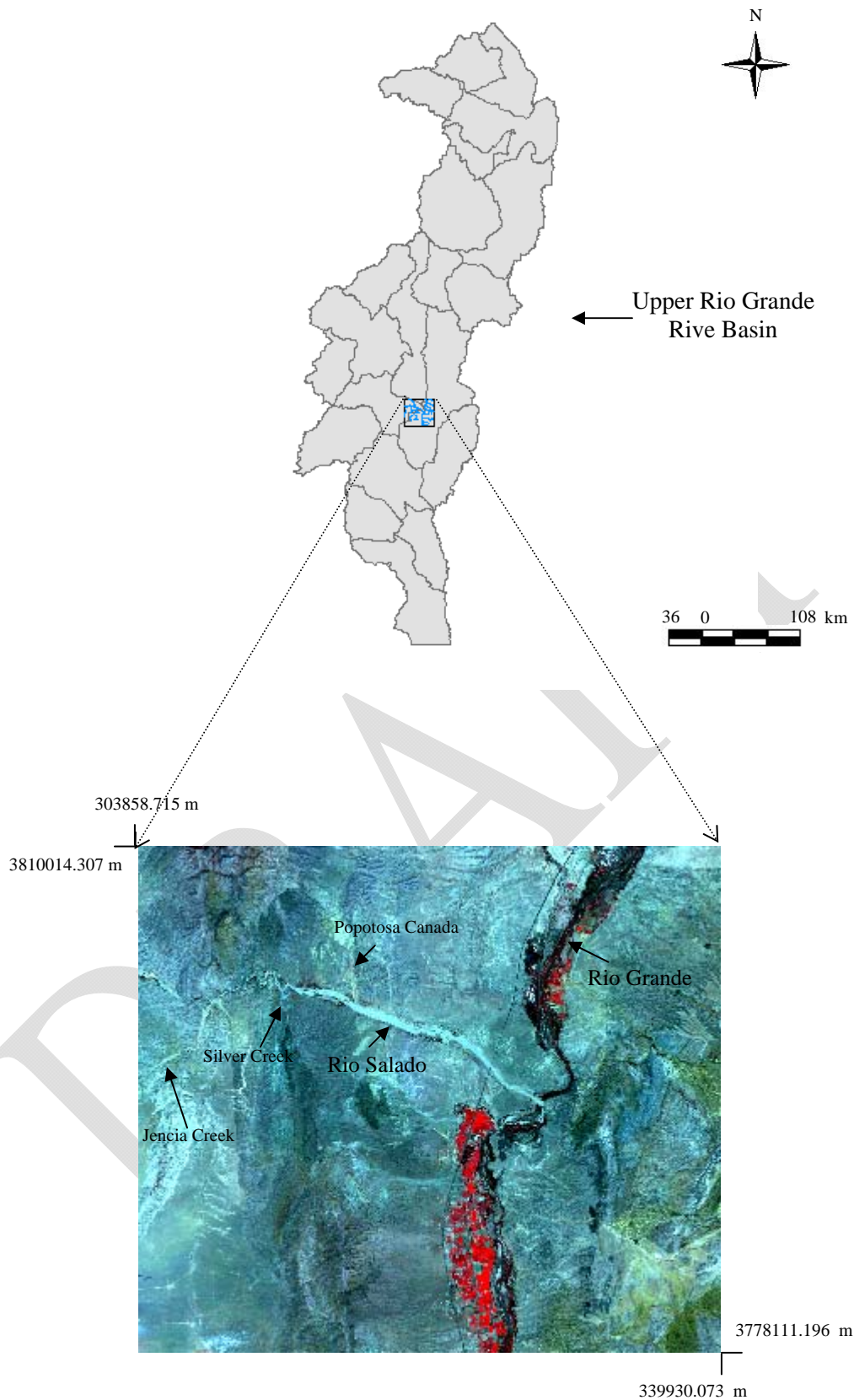


Fig. 2: False colored composite of the area of interest in Upper Rio Grande River basin using bands 3N (0.78-0.86 μm), 2 (0.63-0.69 μm) and 1 (0.52-0.6 μm) of ASTER level 1-B product. Coordinate system: UTM.

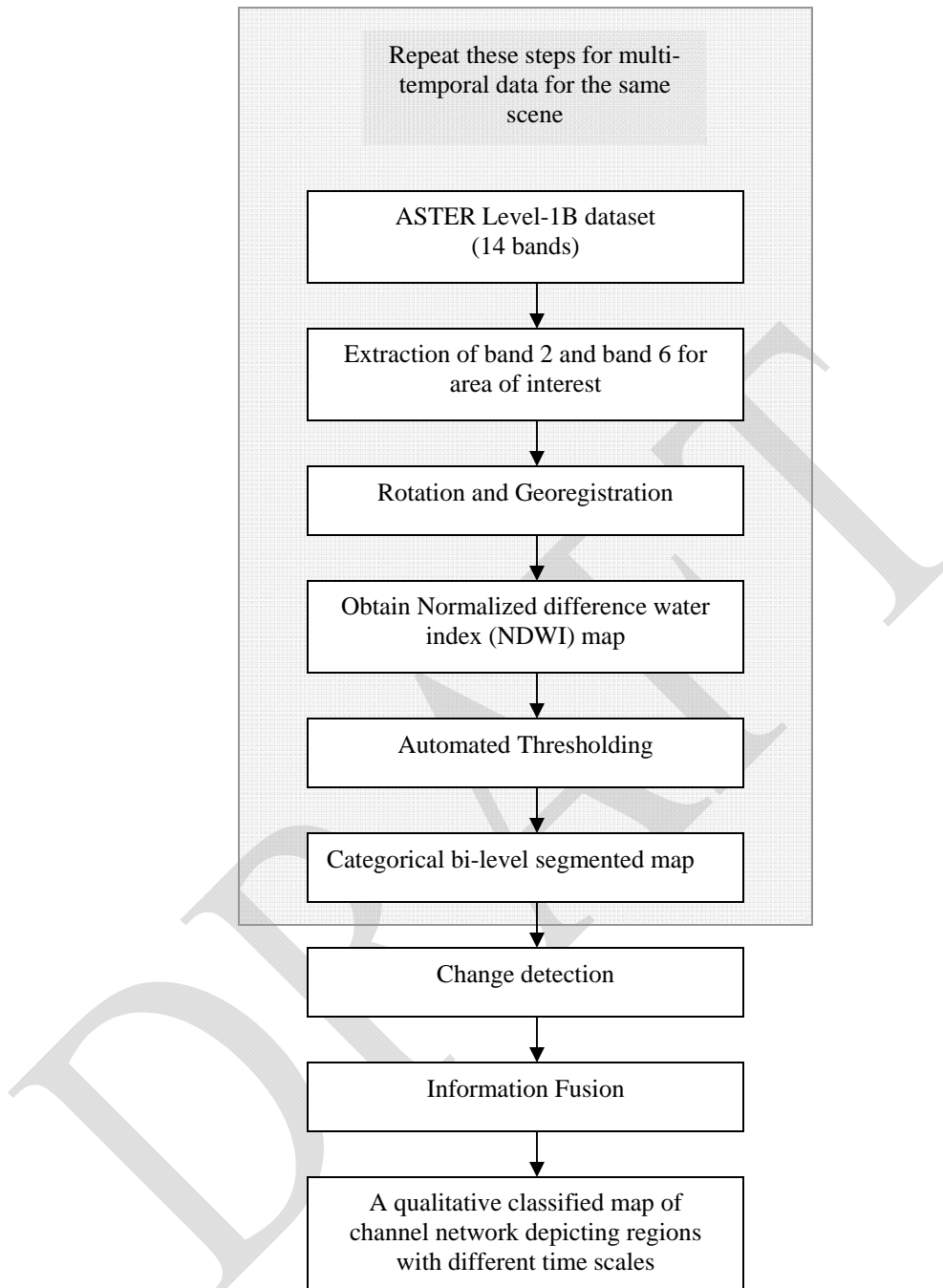


Fig. 3: Flowchart depicting the sequence of steps implemented in the proposed methodology

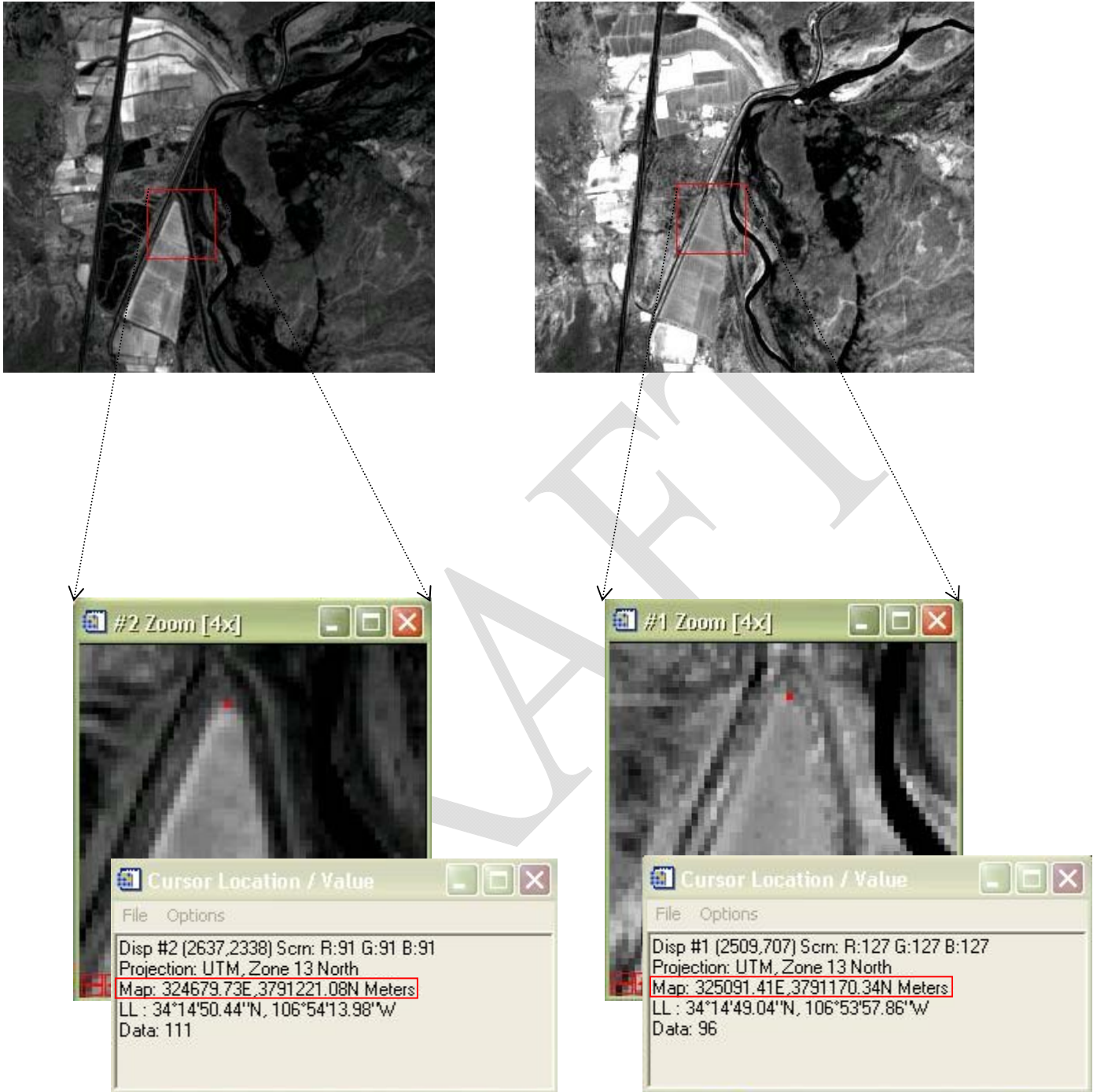


Fig 4: Geometric displacement between two image pairs viz. AST_L1B_003_07192000181741_05132003042026 and AST_L1B_003_04262001180635_01302004133658 is evident even when ASTER level 1B georegistration metadata is used. Red dot shows the corner of the same artificial channel in the image pair. Coordinate value of the red dot in either of the images is shown in “Cursor Location/Value” window.

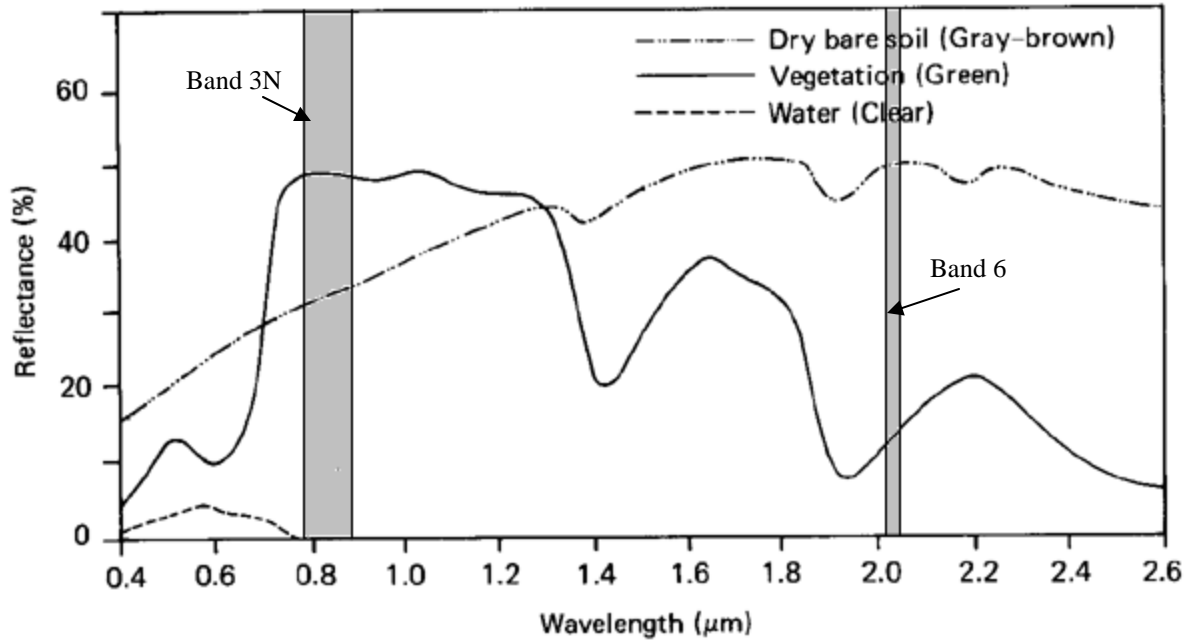


Fig. 5: Spectral signature of some common land cover types along with shaded window depicting the band width band # 3N and 6 respectively of ASTER Level 1B product. Modified from http://geog.hkbu.edu.hk/virtuallabs/rs/env_backgr_refl.htm.

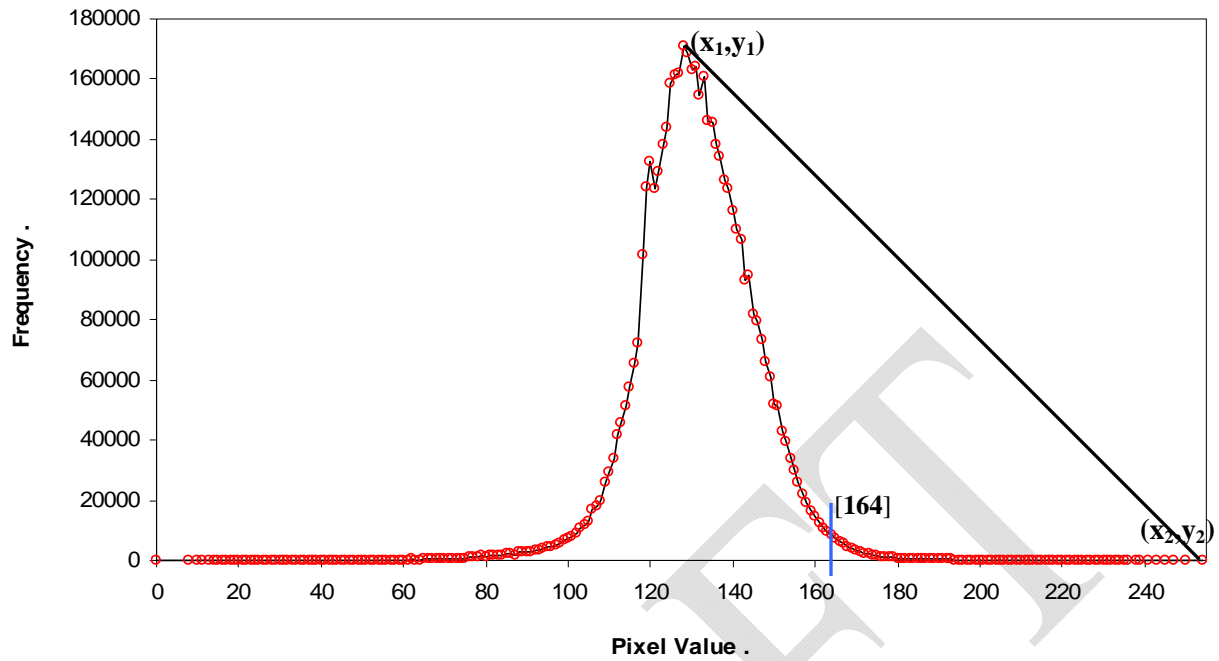


Fig. 6: Unimodal Thresholding applied to an NDWI map obtained from AST_L1B_003_06162002175757_07052002124606. Note that (x_1, y_1) and (x_2, y_2) are the extremes used in eqn (2). Threshold value obtained for this image is 164

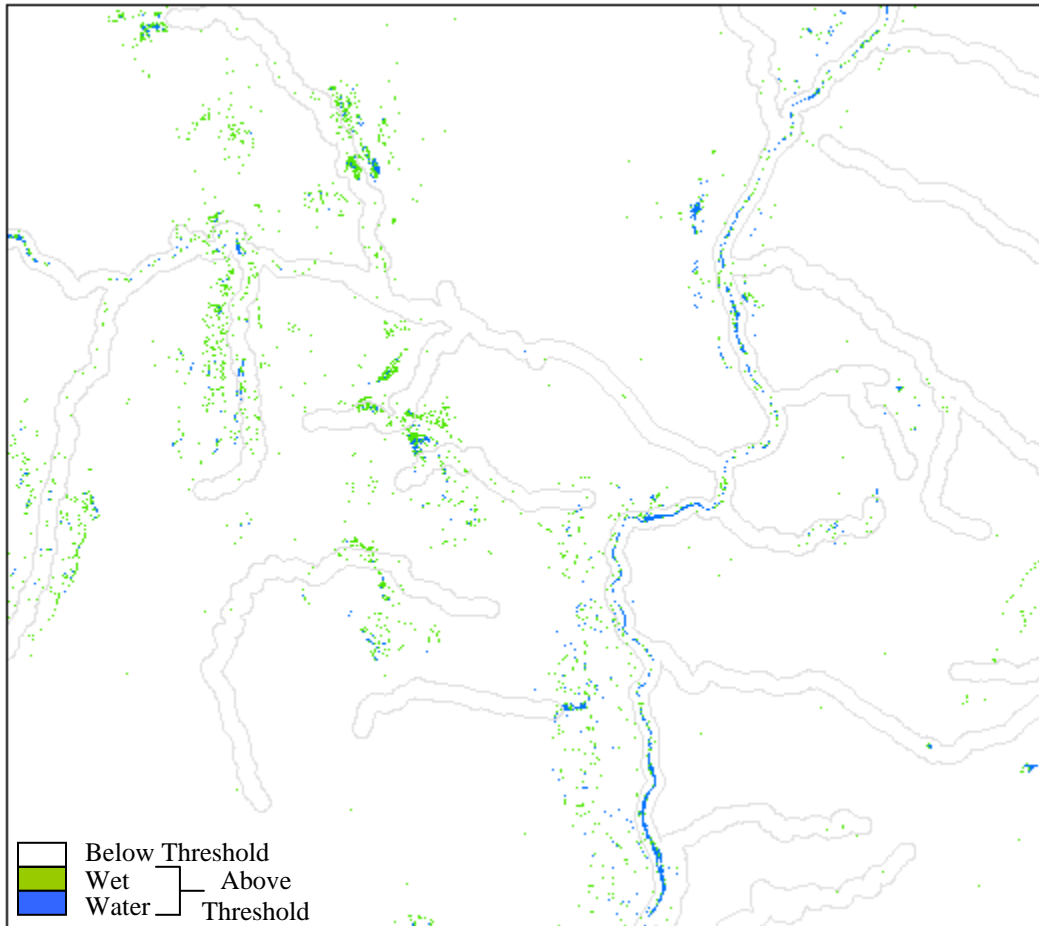


Fig. 7: Bi-level segmented image for image AST_L1B_003_06162002175757_07052002124606. Threshold selected using automated thresholding algorithm was 164. Linear polygonized layer overlaid on the segmented image are the regions with high probability of existence of flow network obtained from DEM (as described in section IV-d).

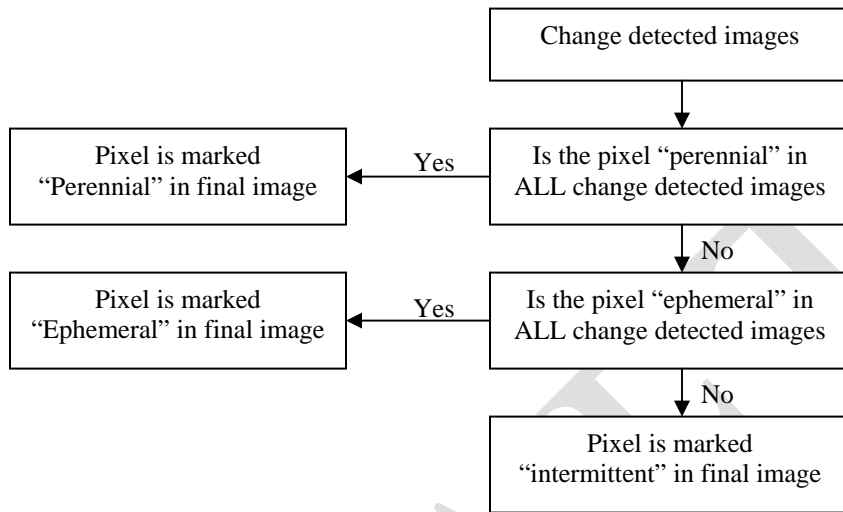


Fig. 8: Information regarding change of a pixel's status (wet or dry) with time is used to categorize a pixel as ephemeral, intermittent or perennial. The decision process is depicted in this graphic.

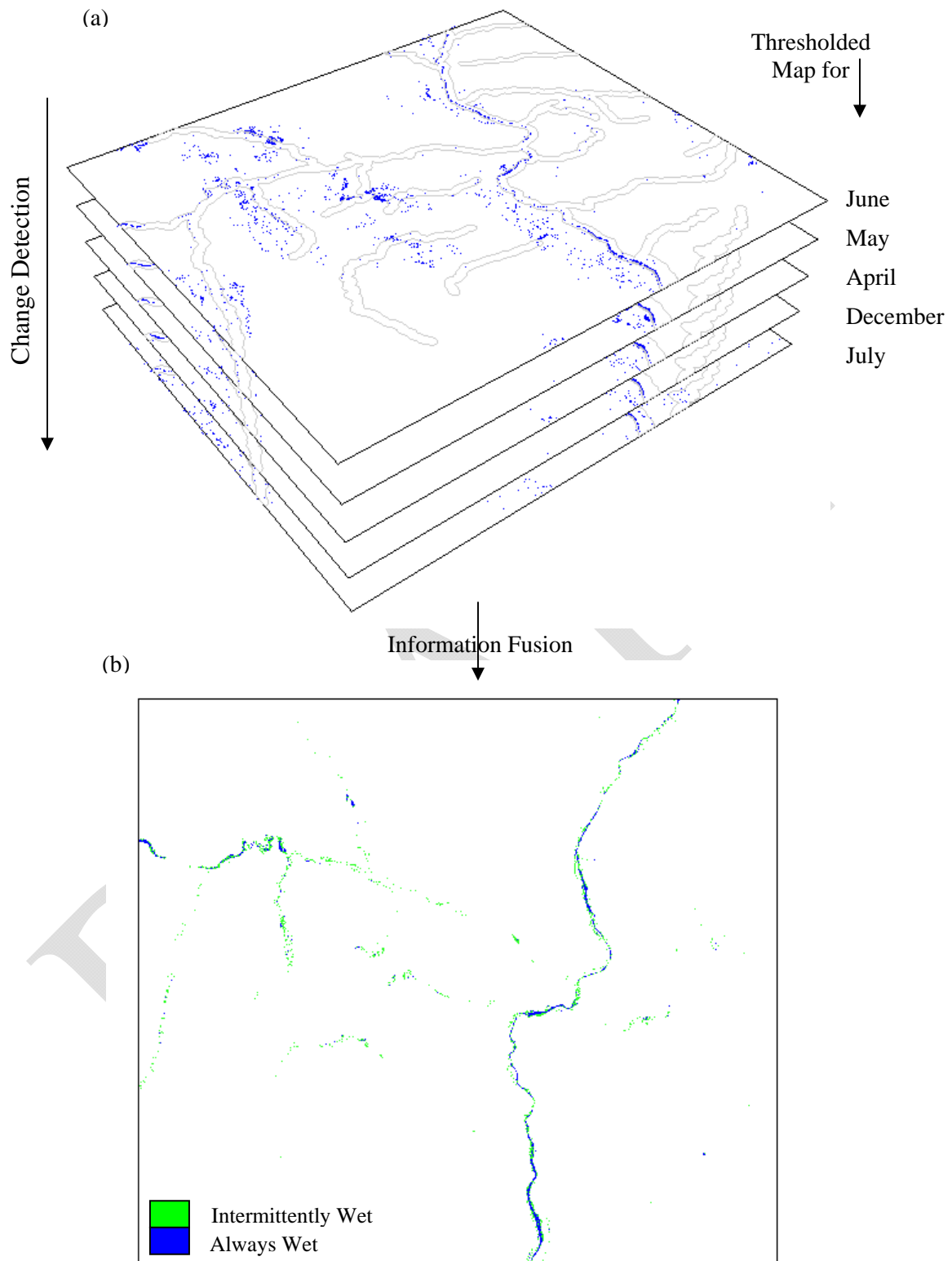


Fig. 9(a): Change detection is performed on multi-temporal thresholded images. Shown above is a pyramid of segmented maps belonging to different months. b) Information about the tracked changes is fused to form a final classified map.

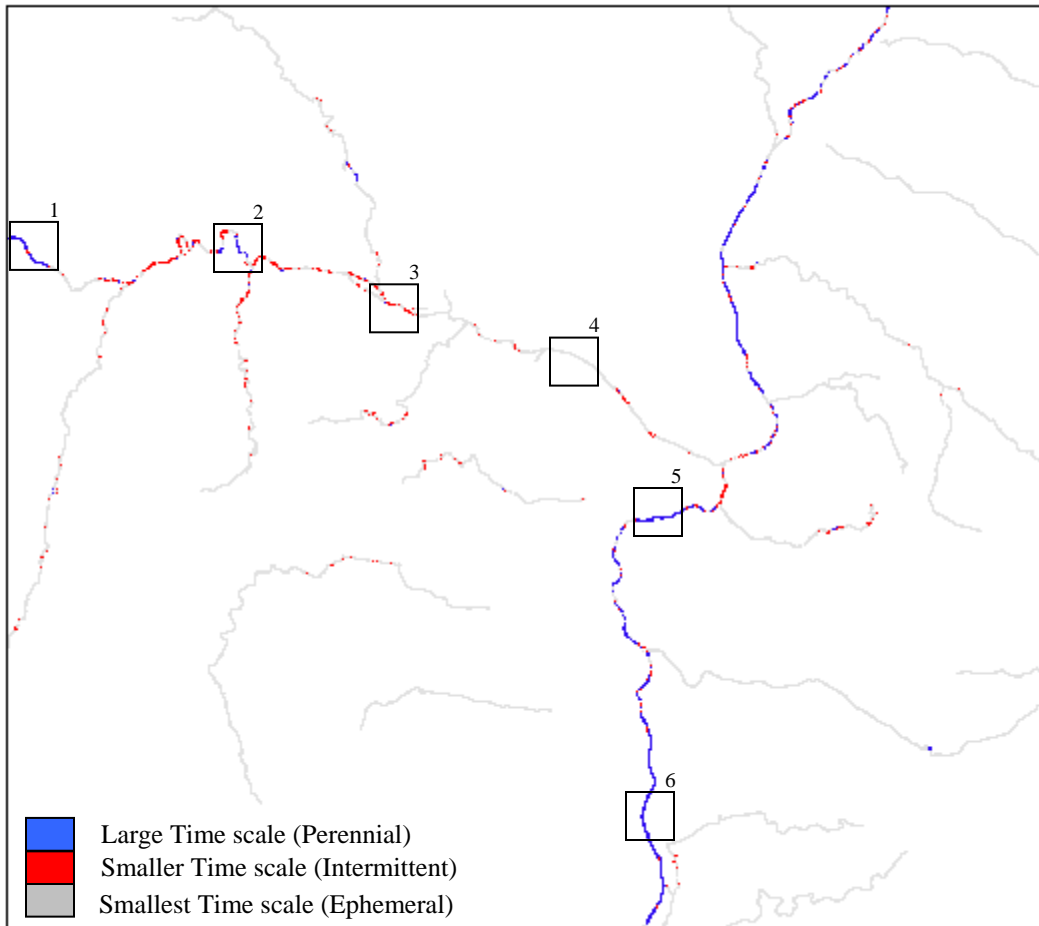


Fig. 10: A qualitative classified channel network depicting the regions with relatively different times scales.

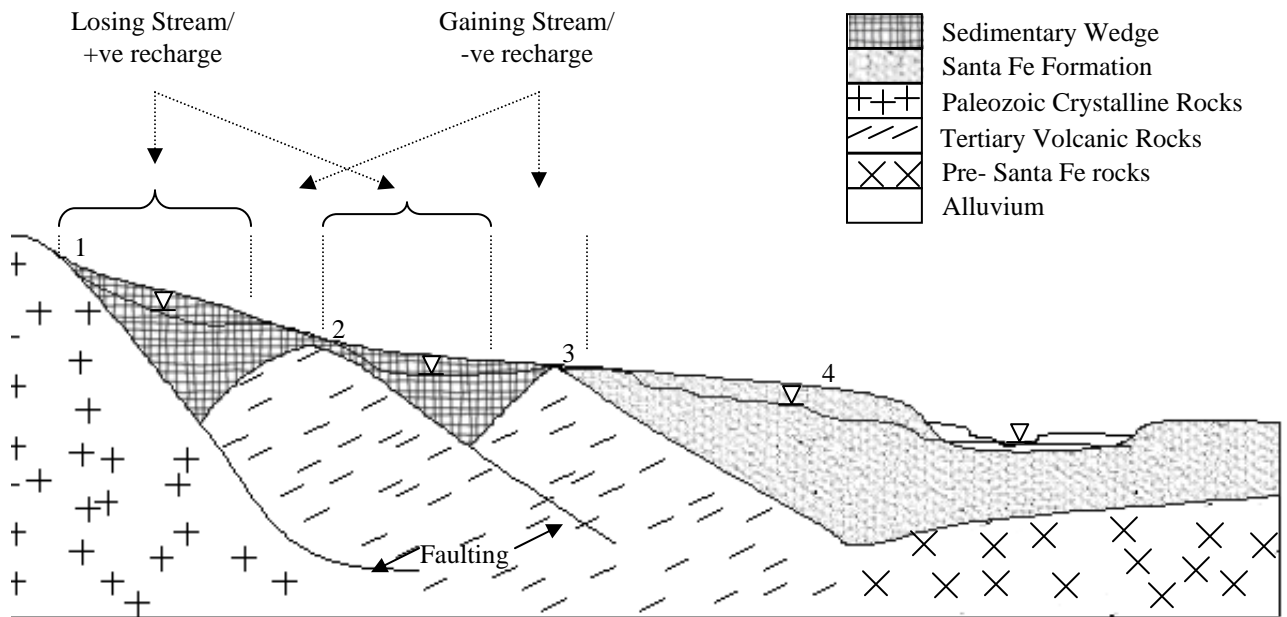


Fig. 11: Geologic structure along a Rio-Salado transect (Modified from Beeson and Duffy, 2004).



Fig. 12: Wet-dry areas obtained from steady-state simulation of Rio-Salado basin using ModHMS (Beeson, 2008)